Coastal Engineering 60 (2012) 69–83

Contents lists available at SciVerse ScienceDirect

Coastal Engineering

journal homepage: www.elsevier.com/locate/coastaleng

Validation of an advective-deterministic approach to short wave breaking in a surf-beat model

Christopher Daly [a,c,*], Dano Roelvink [a,b,c], Ap van Dongeren [a], Jaap van Thiel de Vries [a,c], Robert McCall [a]

[a] Deltares, P.O. Box 177, 2600 MH Delft, The Netherlands
[b] Water Engineering, UNESCO-IHE Institute for Water Education, Westvest 7, 2611 AX Delft, The Netherlands
[c] Department of Civil Engineering and Geosciences, Delft University of Technology, Stevinweg1, 2628 CN Delft, The Netherlands

ARTICLE INFO

Article history:
Received 20 July 2010
Received in revised form 10 August 2011
Accepted 23 August 2011
Available online 28 September 2011

Keywords:
Wave breaking
Wave height
Fraction of breaking waves
Breaker parameter
XBeach

ABSTRACT

An advective-deterministic approach (ADA) to model wave energy dissipation through breaking is presented. This is calibrated against experimental irregular wave data with a high spatial density of surface elevation records using a wave-group-forced surf-beat model, XBeach. In the ADA breaker model, wave breaking is turned on and off by specifying upper and lower values of the breaker parameter (the latter termed wave reforming as in Dally et al. (1985)) and the state of breaking is advected shoreward at the individual wave celerity. For the validation of the proposed ADA model, results are compared with the breaker formulation of Roelvink (1993) using 10 prototype field experiment cases and 32 laboratory flume experiment cases. The ADA breaker model shows good results for short wave height transformation and significant improvement is obtained for the fraction of breaking waves over the Roelvink (1993) formulation, with the modelled data quantitatively and qualitatively representing measurements. It is possible that the ADA wave breaking model could influence other surf zone processes such as low frequency wave generation and nearshore circulation patterns.

1. Introduction

1.1. Overview

Over the past thirty years a number of wave breaking formulations have been proposed which are capable of predicting the energy dissipation of stationary and irregular breaking waves over nearshore topographies. Roelvink (1993) describes three classes of breaking models which are still in use today. Firstly, the parametric models which assume a distribution of wave height, H, and fraction of breaking waves, Q_b, using an estimated RMS wave height, H_{rms}, and breaker parameter, γ (Baldock et al., 1998; Battjes and Janssen, 1978; Thornton and Guza, 1983). Secondly, the probabilistic or wave-by-wave class of models separates the wave height and period distribution offshore into a number of discrete bands and propagates the waves in each band until incipient breaking, where an appropriate parametric dissipation model is applied (Dally, 1990, 1992; Mase and Iwagaki,, 1982). Thirdly, the dynamic class of models operates on time discretization of the propagation of short wave groups (by means of wave action balance equations) and therefore employs a dissipation formulation on the scale of the wave group (Roelvink, 1993; Symonds and Black, 1991). Each class of wave breaking is designed to work well with a respective wave model class: wave-averaged circulation models, wave-by-wave (Boussinesq-type) models and lastly surf-beat (low frequency wave resolving) models with time-varying wave-group forcing.

The breaker formulations of Battjes and Janssen (1978); Thornton and Guza (1983) and Roelvink (1993) are expressed in terms of a probabilistic function. A shortcoming in these breaker formulations is that they tend to smoothen wave breaking over a wide area depending on the local wave height to water depth ratio. Additionally, when these models are applied in the case of varying nearshore bathymetry, for example with a bar-trough system, sudden increases in the water depth immediately after the bar will lower the value of Q_b in the model to values close to zero. This can be interpreted as the instantaneous cessation of breaking. However, in nature, waves tend to break at a specific point and for a given period of time before stabilising and reforming again. After stabilizing and reforming, the wave will propagate further into shallow water until the initial breaking condition is again satisfied and breaking will resume. Dally (1990, 1992) captures this idea of wave breaking being distinctly turned on and off in his proposed wave-by-wave algorithm for random wave breaking.

1.2. Objectives and outline

In this paper we propose, calibrate and validate an advective-deterministic approach (ADA) to determine energy dissipation due to wave breaking which takes into account the history of wave

* Corresponding author at: MARUM, Universitat Bremen, Leobener Strasse, 28359 Bremen, Germany. Tel.: +49 421 218 65582; fax: +49 421 218 65515.
E-mail address: chrisdaly@uni-bremen.de (C. Daly).

0378-3839/$ – see front matter © 2011 Elsevier B.V. All rights reserved.
doi:10.1016/j.coastaleng.2011.08.001

breaking. This breaker model is implemented in a time-varying, process-based, wave-group-forced numerical model, XBeach (Roelvink et al., 2009). In XBeach, short waves are the main forcing mechanism for low frequency waves. The correct physical representation of the short wave shoaling and breaking process is therefore important not only in predicting cross-shore wave height transformation, but is also a key factor in determining radiation stress gradients in the surf zone and hence combined bound and free low frequency wave motions (Longuet-Higgins and Stewart, 1962; Schaffer and Svendsen, 1988; Symonds et al., 1982).

The proposed ADA breaker model is calibrated using error statistics obtained for two key variables (namely the RMS wave-group varying short wave height, H_{rms}, and the time-averaged fraction of breaking waves, Q_b) from the results of a controlled fixed-bed flume experiment (Boers, 1996) to obtain optimised parameter settings. The use of Q_b together with H_{rms} for model calibration is based on the premise that they are both directly synonymous and physically related to energy dissipation through wave breaking but not mutually redundant. The effect of the location of wave gauges in the pre- and post-bar area (outside and inside the main wave breaking zone respectively) is also investigated in the calibration of the proposed breaker model. Subsequent validation tests compare the model results using the calibrated parameter settings of the proposed ADA dissipation formulation with a number of laboratory and prototype test cases and the results using the breaker model of Roelvink (1993). The results of cross-shore H_{rms} and Q_b are highlighted and the model calibration procedure, theory and implications are discussed.

2. Numerical and wave breaking model

2.1. Numerical model description

The numerical model XBeach (Roelvink et al., 2009) is used in the present study to test the proposed wave breaking formulation. XBeach provides a flexible environment for modelling time-varying, depth-averaged nearshore hydrodynamics. Among other routines, the model system consists of a short wave module, which uses time-varying wave action balance equations (including wave shoaling and refraction), given one-dimensionally for the present purpose as:

$$\frac{\partial A}{\partial t}+\frac{\partial c_g A}{\partial x}=-\frac{D}{f} \tag{1}$$

and

$$A(x,t)=\frac{E(x,t)}{f(x,t)} \tag{2}$$

where A is the wave action in space (x), and time (t), f and c_g are the intrinsic wave frequency and wave group celerity obtained from linear theory respectively, and E is the wave energy which varies on the wave group timescale. The total dissipation, D, accounts for frictional dissipation and wave breaking dissipation, the latter including a roller dissipation model (Deigaard, 1993).

A parameterization of the instantaneous energy-based wave-group varying short wave height (hereafter referred to as the 'short wave height') is determined from the short wave energy envelope as:

$$H_E(x,t)=\sqrt{\frac{8E(x,t)}{\rho g}}. \tag{3}$$

The model is forced by a time series of a wave-group varying short wave energy envelope that can be computed from defined JONSWAP spectral parameters or measured wave height time series. Roelvink et al. (2009) provide further detail and explanation of boundary condition forcing in XBeach.

2.2. Review of Battjes and Janssen (1978) and Roelvink (1993)

Bore-based wave dissipation formulations, where the energy dissipation in a wave is similar to that in a hydraulic jump (Le Mehaute, 1962), were first applied to models which compute time averaged wave breaking dissipation by Battjes and Janssen (1978) (hereafter referred to as BJ78). BJ78 expressed the average energy dissipation by wave breaking, D, as the product of two variables. Firstly, the energy dissipation rate, D_b, of a breaking wave, is defined as a function of the (Rayleigh) distribution of wave heights. Secondly, the (time-averaged) probability, Q_b, that waves above a certain maximum height, H_b, are breaking relative to a local RMS wave height to water depth ratio, was termed the breaker parameter γ. This is expressed as:

$$\langle D\rangle=\langle Q_b\rangle\langle D_b\rangle \tag{4}$$

with

$$\langle D_b\rangle=\frac{\alpha}{4}\rho g f\frac{{H_b}^3}{h} \tag{5}$$

and

$$\frac{1-\langle Q_b\rangle}{\ln\langle Q_b\rangle^{-1}}=\left(\frac{H_{rms}}{H_b}\right)^2 \tag{6}$$

where

$$H_b=\gamma h \tag{7}$$

and where α is a factor which generally represents the intensity of wave dissipation, f is the intrinsic wave frequency and $\langle\cdots\rangle$ denotes time-averaged values. Battjes and Stive (1985) did extensive calibration and verification of the Battjes and Janssen (1978) model and Thornton and Guza (1983) revised the probability distribution function based on field data. Baldock et al. (1998) also revised the Thornton and Guza (1983) version to account for unsaturated surf zone conditions.

The dissipation formulations of BJ78, Thornton and Guza (1983) and Baldock et al. (1998) are widely applicable to wave averaged models. They may also be used to simulate the breaking of regular wave groups in dynamic models, however the pre-definition of H_{rms} in the formulation of Q_b makes it inappropriate to use in the time-dependent dissipation of energy in irregular wave groups. Doing so would imply that breaking is dependent on a predefined long term parameter rather than one which varies over the localised wave group timescale (Roelvink, 1993).

Roelvink (1993) (hereafter referred to as Rv93) eliminated the dependency of Q_b on a specified RMS wave height by introducing a dissipation formulation fundamentally based on the wave energy. It is implemented within the dynamic class of numerical models which operates on the timescale of wave groups. Rv93 re-expresses D_b in a time-varied form as:

$$D_b=\frac{\alpha}{4}\rho g f{H_b}^2 \tag{8}$$

where H_b is assumed to be in the same order as the water depth ($\approx$1), therefore reducing the cubic power in Eq. (5) to a square power in Eq. (8). The definition of Q_b in Eq. (6) is changed from a time-averaged probability of breaking to an instantaneous probability of breaking, which is termed P_b to avoid confusion and is expressed as:

$$P_b=1-\exp\left[-\left(\frac{H_E}{\gamma h}\right)^n\right] \tag{9}$$

where n is a shape factor usually of value 10 and H_E is the (energy-based) short wave height. Rv93 uses Eq. (4) as a base to rewrite it as:

$$D = P_b D_b. \tag{10}$$

The Rv93 model, though applicable to dynamic wave-group-forced numerical models, uses the localised ratio of H_E/h to predict the probability of breaking, which ignores the history of wave breaking itself (i.e. breaking is not tracked).

2.3. Proposed approach to wave breaking

Dally et al. (1985) present a model for wave dissipation of regular waves and are the first to make use of a wave stability coefficient to account for wave reforming after breaking. Dally (1990, 1992) uses the same concept of wave dissipation applied to a wave-by-wave modelling approach whereby criteria for incipient breaking and the amount of energy dissipation during breaking is specified. The concept of simulating the natural process of breaking being turned on and off can also be transferred to an energetic approach where the irregular short wave height (H_E) is modelled. This is achieved by changing the probability function in Eq. (9) to represent wave breaking as being deterministic: i.e. either a wave is breaking or it is not. Therefore, while it is possible to have values of Q_b or P_b anywhere between 0 and 1 in the BJ78 or Rv93 models for example, in the proposed breaker model the *state of breaking*, now introduced as B to avoid confusion, only has binary values (0 or 1). In the proposed breaker model, breaking occurs when $H_E > \gamma_b h$ and stops breaking when $H_E < \gamma_r h$, where γ_b and γ_r are termed the breaker and reformation parameters respectively, and may be expressed as:

$$\gamma_b = \frac{H_{E,b}}{h} \quad \text{and} \quad \gamma_r = \frac{H_{E,r}}{h}. \tag{11}$$

For values of H_E between both limits the property that wave breaking occurs (or not) propagates with the individual wave celerity, c_x. We can formulate this as follows:

$$B = 1, H_E > \gamma_b h \tag{12}$$

$$\frac{\partial B}{\partial t} + c_x \frac{\partial B}{\partial x} = 0, \gamma_r h < H_E < \gamma_b h \tag{13}$$

$$B = 0, H_E < \gamma_r h. \tag{14}$$

We also rewrite Eq. (4) as:

$$D = BD_b. \tag{15}$$

With this algorithm, we follow the waves (i.e. the short wave height, H_E) as they are coming from offshore; they shoal (with $B=0$) until H_E exceeds the breaking criterion. They then break ($B=1$) and keep breaking until H_E becomes less than the reformation criterion. The differential in Eq. (13) is used to advect B shoreward, and therefore requires a time-domain numerical model in order to function. The advection of B ensures that the history or memory of wave breaking is maintained for its duration (while $B=1$). This tracking of wave breaking ensures that premature wave breaking does not occur.

Fig. 1 shows an example of how the proposed approach to wave breaking functions in a dynamic, wave-group forced numerical model using a bar–trough nearshore bathymetry. In this example, a time stack of the cross-shore variation of H_E is shown as well as areas where breaking is occurring ($B=1$). It is shown in the first time stack $t=1$ s that breaking starts (at 14 m distance) when the local H_E becomes unstable (the local γ exceeds a given γ_b threshold). Breaking is advected towards the shore at the speed c_x, (illustrated by the black dotted line and red circles). Breaking is also shown to occur as the highest waves in the group (the crests of H_E) pass over the bar. Breaking continues for some time until H_E becomes stable again at $t=8$ s (the local γ falls below a given γ_r threshold) after passing some distance from the bar. Breaking reoccurs again at $t=9$ s as the wave envelope moves further into shallow water, again forcing the local γ to exceed the given γ_b threshold. Fig. 1 also shows that the position of the breakpoint is able to fluctuate in time, therefore at any given time there may be one or more locations where waves are breaking (e.g. at $t=10$ s and $t=3$ s respectively). The time-averaged fraction of breaking (Q_b) at a specific location can be determined by simply finding the time-average of B at that point over the simulation period, hence, $Q_b = \langle B \rangle$. This is comparable to the time-averaged Q_b in other breaker formulations such as BJ78 and Rv93.

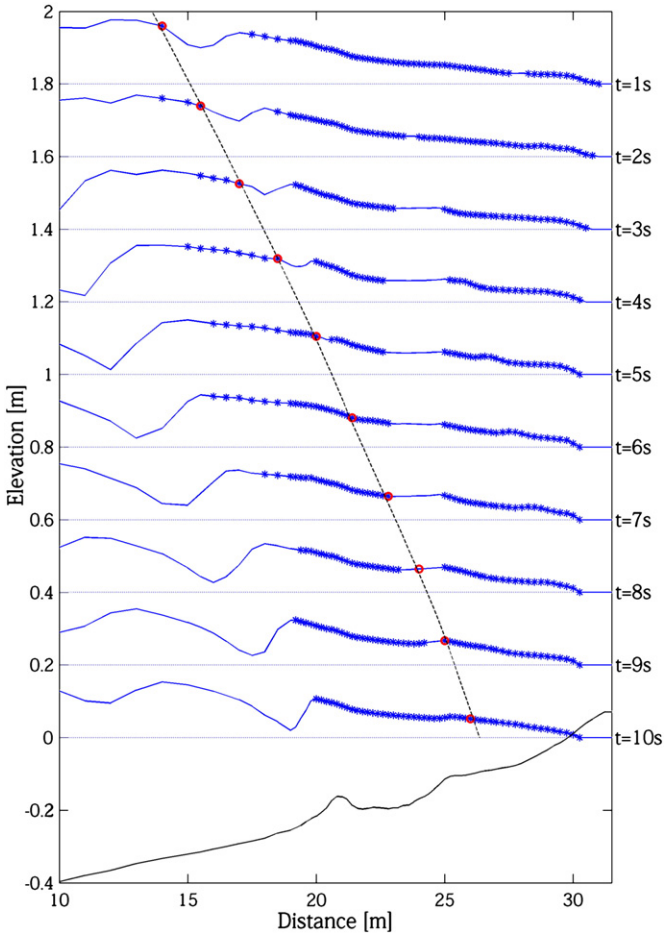

Fig. 1. An example of the ADA wave breaking model applied to a bar–trough bathymetry (black —). A time stack of the cross-shore profile of the wave-group varying wave height, H_E (blue —), shows areas where the wave is breaking (blue *). The individual wave celerity profile (black —) indicates the advection of the first breakpoint of the incoming wave (red ○).

This combined advective-deterministic approach (ADA) to wave breaking, given by the equation set (5), (12), (13), (14) and (15), is implemented in the time-varying wave-group-forced numerical model, XBeach (together with the Rv93 breaker formulation) and is the subject of the calibration and validation in this paper.

3. Model calibration

3.1. Calibration experiment

The controlled flume experiments of Boers (1996) (hereafter Boers) are used for calibration of the ADA model as it features

irregular waves propagating over a bar–trough bathymetry. These experiments are ideal for the calibration of the model parameters as waves are allowed to reform after passing over the bar. Boers conducted his experiments in the 40 m long wave flume of the Fluid Mechanics Laboratory at Delft University of Technology. The offshore water depth in the flume is kept at 0.75 m and the flume width is 0.8 m. The flume is equipped with a piston-type wave generator which is capable of active reflection compensation (ARC), which absorbs reflected (long) waves, and has second order (Stokes) wave steering.

The experiment has a high spatial density of wave gauges in order to obtain a high resolution of the short wave breaking process in shallow water. The fixed bathymetry in the experiment, featuring a bar–trough formation in the nearshore, is reproduced and scaled from the LIP 11D experiments carried out in the Delta Flume (Roelvink and Reniers, 1995) starting 5.0 m from the wave generator. The first wave gauge is located at the toe of the sloping bathymetry (referenced as $x=0$ m). The gauge spacing varies from 1.0 m in the deepest section of the flume to 0.25 m around the breaker bar. In total, there are 70 locations with wave signal data over a distance of 28.5 m. The sampling frequency of the wave measuring instruments is 20 Hz. The bathymetry and location of the wave gauges are shown in Fig. 2.

The irregular wave cases of Boers are defined using a parameterized JONSWAP spectrum. In his experiments, Boers used three wave conditions, named series 1A, 1B and 1C (taken from the LIP 11D experiments). 1A and 1B have the highest f_p values; however, 1B has the highest H_{m0} value and therefore the most extreme wave steepness. Series 1A and 1C follow in decreasing order in terms of steepness, with the latter having the longest period waves. Wave breaking observed during 1B started very early in the flume, whereas in 1C shoaling of the waves occurred over the outer bathymetry with minimal breaking until the waves reached the outer bar. The JONSWAP spectral parameters for these irregular wave cases are given in Table 1. All experiments were carried out with a spectral peak enhancement factor of 3.3.

3.2. Procedure

The calibration of the parameters which affect short wave breaking for the ADA model (γ_b, γ_r, and α) is done by running several numerical computations of the wave flume conditions of the Boers 1A and 1B flume experiments using XBeach. For these model runs γ_b, and γ_r are varied systematically within ranges from 0.40 to 0.58 and 0.24 to 0.39 respectively with a step size of 0.03. The parameter α in Eq. (5) is initially kept at a constant value of 1.0, a commonly accepted value (Baldock et al., 1998; Battjes and Janssen, 1978 and Roelvink, 1993). The sensitivity of γ_b, and γ_r to varied α values is investigated thereafter.

From the model output, the RMS (over time) of the short wave height, H_E (termed H_{rms}) and the time-average of the state of breaking, B, (termed Q_b, equivalent to the fraction of breaking) are compared with measured data to obtain several error statistics. The output variables (H_{rms} and Q_b) used for comparison with the measured data are directly related to short wave shoaling and breaking and can therefore be used to calibrate the ADA model parameters (γ_b, and γ_r).

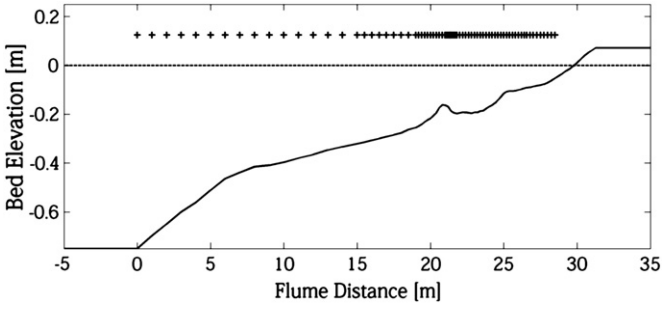

Fig. 2. Bathymetry (—), still water level (—) and wave gauge locations (+) in the flume experiment of Boers (1996).

Table 1
Parameters for Boers wave cases.

Dataset	Series	f_p (Hz)	T_p (s)	H_{m0} (m)
Boers'96	1A	0.476	2.10	0.160
"	1B	0.476	2.10	0.220
"	1C	0.294	3.40	0.107

Estimates of the ADA model performance are computed using relative bias and a scatter index given respectively as:

$$\varepsilon_{bias} = \frac{\langle c-m \rangle}{\max(rms_m, \langle m \rangle)} \tag{16}$$

$$\varepsilon_{scatter} = \frac{rms_{c-m}}{\max(rms_m, \langle m \rangle)} \tag{17}$$

where c and m are the computed and measured data respectively, rms is done over space and $\langle \cdots \rangle$ denotes space-averaging. The relative bias and scatter are the normalised raw average and RMS error respectively; therefore results which give the least bias and scatter are the most favourable. Each error statistic is sensitive to the relative "one-on-one" distribution of measured and computed data. For instance, it is possible to have relatively low bias but high scatter, or vice versa. Raw error values (ε_{bias} and $\varepsilon_{scatter}$) are obtained for the variables H_{rms} and Q_b using Eqs. (16) and (17). We can also create an ensemble average of the bias and scatter for a combination of each variable (H_{rms}&Q_b). For the combined variable error values, equal weight is given to both variables H_{rms} and Q_b and expressed as:

$$\langle \varepsilon_{bias} \rangle = \langle |\varepsilon_{bias}(H_{rms})| + |\varepsilon_{bias}(Q_b)| \rangle \tag{18}$$

$$\langle \varepsilon_{scatter} \rangle = \langle \varepsilon_{scatter}(H_{rms}) + \varepsilon_{scatter}(Q_b) \rangle \tag{19}$$

where $|\cdots|$ denotes the modulus. Since we are interested in the composite minima of both the bias and scatter errors themselves in order to find the optimal values of the ADA model parameters (γ_b, and γ_r), we further average the (absolute) error values of both error statistics. Equal weight is given to each error statistic in the final result, such that:

$$\langle \varepsilon_{composite} \rangle = \langle \langle \varepsilon_{bias} \rangle + \langle \varepsilon_{scatter} \rangle \rangle \tag{20}$$

(cf. van der Westhuysen, 2010). The lowest error value from the error distribution obtained using Eq. (20) defines the optimal values of γ_b, and γ_r. From the several optimal parameter values obtained for the different variable combinations, a final set of calibrated parameter values is then specified for γ_b and γ_r which is later used to validate the ADA model.

In order to investigate the differences between the physical processes of wave shoaling and breaking, the flume is subdivided into two sections: a pre- and post-bar area. The pre-bar area is seaward of the crest of the nearshore breaker bar ($0<x<21$ m), which includes the area where waves shoal and subsequently begin to break. The post-bar area is located shoreward of the crest of the breaker bar ($21.1<x<28$ m) and has the greatest occurrence of wave breaking (not less than 25% breaking waves, refer to Fig. 11 in Section 4.3). This division of the flume area results in 34 of the 70 wave gauge locations being allocated to the pre-bar zone and the remaining 36 to the post-bar zone.

3.3. Results

3.3.1. Optimal γ_b and γ_r values

Fig. 3 shows how the raw error distribution of the bias and scatter of the RMS short wave height results for case Boers 1A, $\varepsilon_{bias}(H_{rms})$ and $\varepsilon_{scatter}(H_{rms})$ obtained using Eqs. (16) and (17), gives the composite error distribution, $\varepsilon_{composite}(H_{rms})$ obtained using Eq. (20). $\varepsilon_{bias}(H_{rms})$ and $\varepsilon_{scatter}(H)$ are shown in the first two rows of the figure while $\varepsilon_{composite}(H_{rms})$ is shown in the bottom row. In Fig. 3 the locations of minima are highlighted on the $\varepsilon_{composite}(H_{rms})$ plots, which reveal the optimal point for γ_b, and γ_r (based on calibration with H_{rms} only). Fig. 4 shows the composite error distribution for calibration with Q_b and the H_{rms} & Q_b combination for Boers 1A while Fig. 5 shows the calibration with H_{rms}, Q_b and H_{rms}&Q_b for Boers 1B, all with the minima highlighted. In Fig. 3, Fig. 4 and Fig. 5, the columns show the difference in results obtained when all wave gauges are considered (left) or only those in the pre-bar zone (centre) or post-bar zone (right). The different optimal values of γ_b and γ_r for all calibration runs (H_{rms}, Q_b and H_{rms}&Q_b) using Boers 1A and Boers 1B data are shown in Table 2 in the columns marked'γ_b'and'γ_r'.

The centre column plots of Fig. 3, Figs. 4 and 5 indicate that γ_r has very limited effect on the RMS short wave height in the pre-bar area, as the bias, scatter and their composite error are relatively independent of the value of γ_r, which results in no definitive calibration value for it (also reflected in Table 2). This is because the likelihood of wave breaking is very low in the pre-bar area (Q_b<0.1 for Boers 1A and Q_b<0.2 for Boers 1B) (refer to Fig. 11 in Section 4.3) which consequently means that wave reformation does not occur there frequently enough. Slightly higher levels of breaking (and reformation) results in an apparent minima in γ_r as reflected in the pre-bar plots of Boers 1B in Fig. 5, however, the occurrence of breaking (and reformation) is still too low for reliable calibrated γ_r values. The most sensitive parameter in the pre-bar zone in the ADA model is then γ_b, which controls the onset of breaking and thus regulates the short wave height in the pre-bar area. In the post-bar zone, γ_r has greater influence on the short wave height in shallow water as the surf zone approaches a greater degree of saturation with γ_b, still being an important parameter to ensure that breaking is repetitive.

Based on previous work (Horikawa and Kuo (1966)), γ_r tentatively lies in the range of 0.35–0.40. From the calibration using the Boers wave cases, we see that values of γ_r range from 0.30 to 0.36. For γ_b,

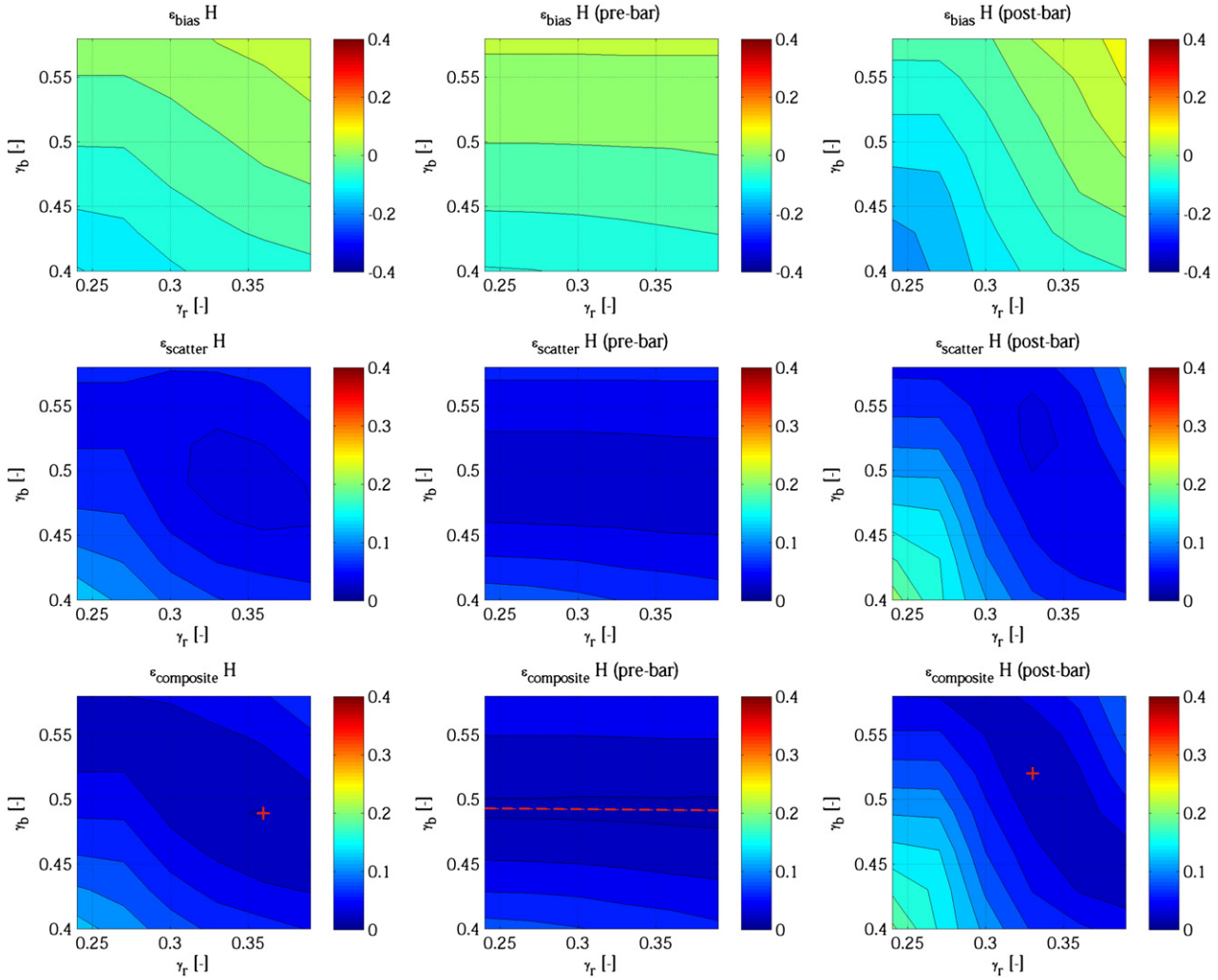

Fig. 3. RMS short wave height raw bias error distribution, $\varepsilon_{bias}(H_{rms})$ (top row), raw scatter error distribution, $\varepsilon_{scatter}(H_{rms})$ (centre row) and composite error distribution, $\varepsilon_{composite}(H_{rms})$ (bottom row) for all wave gauge locations (left column), pre-bar wave gauges (centre column) and post-bar wave gauge locations (right column) from case Boers 1A. Error distribution values (colour scale) are plotted against the breaker parameter, γ_b (vertical axis) and the reformation parameter, γ_r (horizontal axis). Nodes (red +) and axes (red —) of minima correspond to values in Table 2.

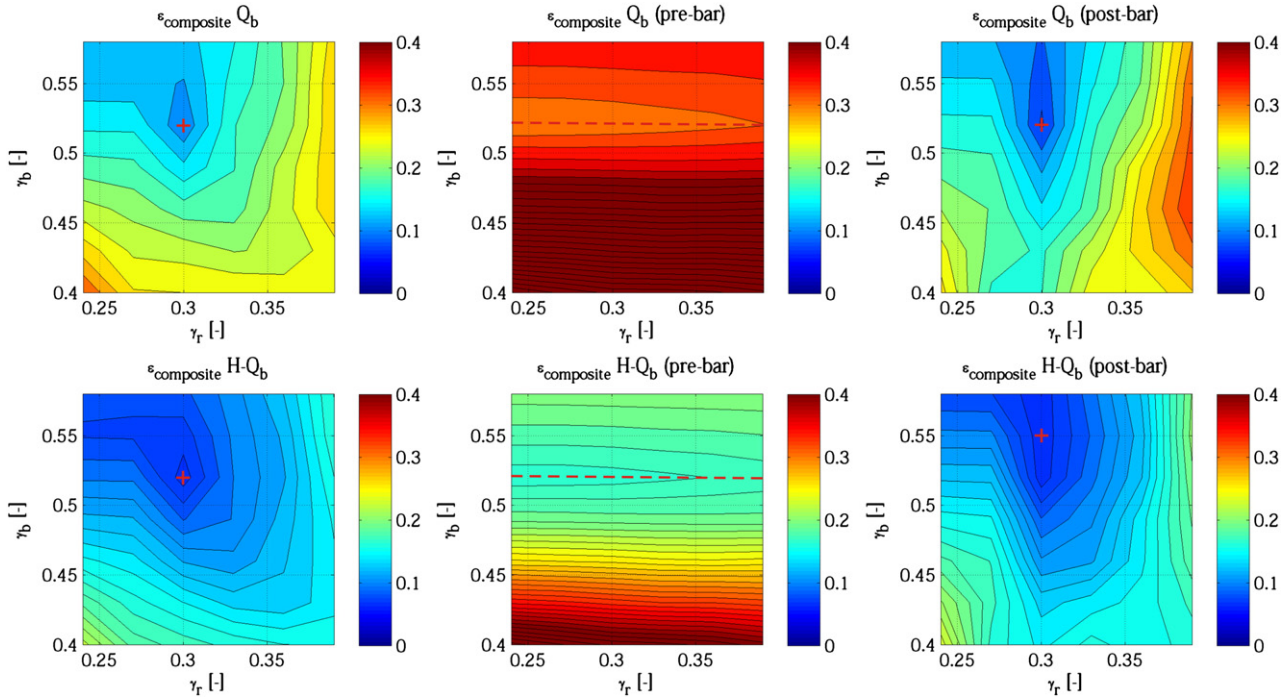

Fig. 4. Composite error distribution for fraction of breaking waves, $\varepsilon_{composite}(Q_b)$ (top row), and the $H_{rms}\&Q_b$ pair, $\varepsilon_{composite}(H_{rms}\&Q_b)$ (bottom row), for all wave gauge locations (left column), pre-bar wave gauges (centre column) and post-bar wave gauge locations (right column) from case Boers 1A. Error distribution values (colour scale) are plotted against the breaker parameter, γ_b (vertical axis) and the reformation parameter, γ_r (horizontal axis). Nodes (red +) and axes (red —) of minima correspond to values in Table 2.

the range of values varies from 0.49 to 0.55, which lie in a similar range as determined by Rv93. The location of corresponding minima of γ_b and γ_r are shown in Fig. 6 for all calibration runs. In the figure, the scatter of the points imply that there is still some variance in wave breaking limits which indicates that the wave breaking process is not completely deterministic. However, it is still within a reasonable range and shows some measure of central tendency. Using prescribed calibrated parameter values for γ_b and γ_r of 0.52 and 0.30 respectively is recommended considering that the calibration result for the most representative case ($\varepsilon_{composite}(H_{rms}\&Q_b)$ using all wave gauges) is similar for both the Boers 1A and 1B experiments (addressed further in the Discussion).

3.3.2. Sensitivity of γ_b and γ_r to varied α values

The prescribed values of γ_b and γ_r given above are determined using a value of α equal to 1.0. Therefore for different values of α, the possible range of values for γ_b and γ_r is likely to change. The sensitivity of γ_b and γ_r is investigated by varying α within a range from 0.6 to 1.6 with a step size of 0.2. A similar evaluation as carried out above is done to determine optimal γ_b and γ_r values for each value of α based on $\varepsilon_{composite}(H_{rms}\&Q_b)$ values. These results are summarised in Table 3.

Table 3 shows that as α is increased, γ_r consistently decreases in value. This is because an increased intensity of dissipation will force γ_r to assume lower values in order to sustain the observed frequency of breaking, albeit at the expense of underestimating the RMS short wave height in the nearshore. γ_b also tends to decrease with increasing a, which implies that for a greater level of dissipation breaking would tend to start earlier. The $\varepsilon_{composite}(H_{rms}\&Q_b)$ values shown in Table 3 indicate the accuracy of the model results for the different values of α. It clearly shows that using a value of α equal to 1.0 gives the best results (lowest error, shown in italics), which is in keeping with the findings of previous studies (Baldock et al., 1998; Battjes and Janssen, 1978 and Roelvink, 1993). Moderate results are obtained when using α values of 0.8 or 1.2, but values outside this range yield rather poor results, most notably in the estimation of Q_b.

Fig. 7 illustrates the result of varying α and γ_r using a fixed γ_b value of 0.52 as obtained in the calibration above. Here it is shown more clearly that optimal α and γ_r values are 1.0 and 0.3 respectively. Similar figures are obtained when the optimal values of γ_r in Table 3 are held constant and α is plotted against γ_r. Therefore, from this analysis, a value of 1.0 for α is strongly recommended for use with the ADA model.

4. Model validation

4.1. Field and experimental datasets

A number of datasets combining both field and laboratory measurements are used for the validation of the ADA model. A total of 10 field cases from 2 datasets and 32 flume cases from 6 datasets are used, all of which include measurements of short wave heights among other variables. The field experiments include 9 cases from the Duck '85 photo-pole measuring campaign (Ebersole and Hughes, 1987) in the United States and one photo-pole experiment conducted by Hotta and Mizuguchi (1980) in Japan. The flume experiments include 8 cases from Van der Meer (1990); 8 cases from Battjes and Janssen (1978); 7 cases from the large scale LIP11D Delta Flume experiments (Roelvink and Reniers, 1995); 6 cases from Van Noorloos (first presented in Van Dongeren et al., 2007); 2 cases from Stive (1985); and lastly, 1 case from Boers (1996). Rv93 gives a description of the field datasets and the flume experiments of Van der Meer, Battjes and Janssen and Stive. Table 4 and Table 5 give the names of the wave cases considered in the field and laboratory experiments respectively as well as the corresponding bathymetry. These tables also indicate the surf condition for each case using the Iribarren number, ξ (Battjes, 1974; Elfrink and Baldock, 2002).

4.2. Procedure

All 10 field cases and 32 flume cases mentioned above are used in the validation of the ADA breaker model using the prescribed parameter

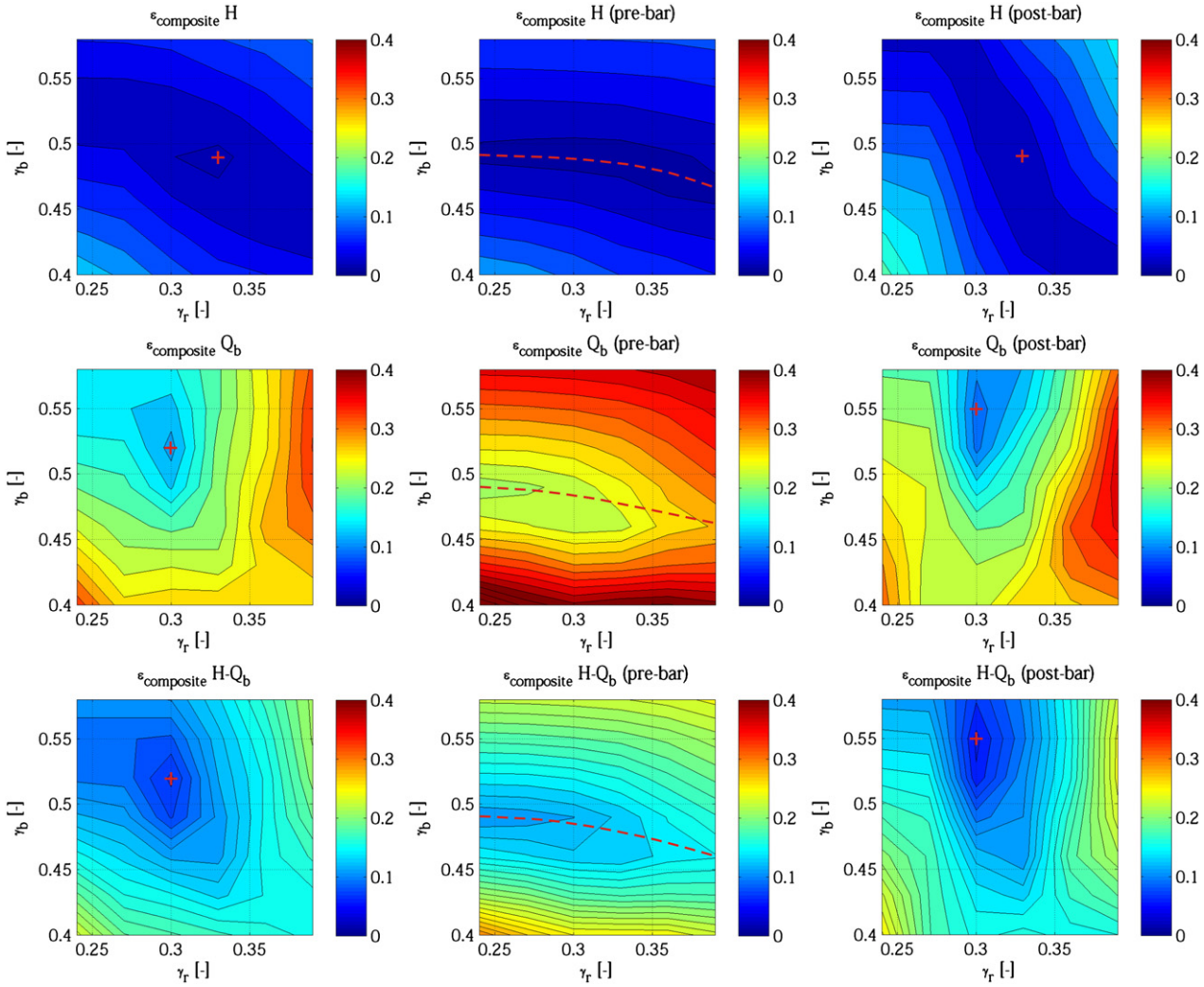

Fig. 5. Composite error distribution for RMS short wave height, $\varepsilon_{composite}(H_{rms})$ (top row), fraction of breaking waves, $\varepsilon_{composite}(Q_b)$ (centre row), and the H_{rms}&Q_b pair, $\varepsilon_{composite}(H_{rms}\&Q_b)$ (bottom row), for all wave gauge locations (left column), pre-bar wave gauges (centre column) and post-bar wave gauge locations (right column) from case Boers 1B. Error distribution values (colour scale) are plotted against the breaker parameter, γ_b (vertical axis) and the reformation parameter, γ_r (horizontal axis). Nodes (red +) and axes (red —) of minima correspond to values in Table 2.

values of γ_b and γ_r from the calibration as 0.52 and 0.30 respectively. This is done in two ways. Firstly, the sensitivity of the calibration parameter values is determined by computing the distribution of raw error values (ε_{bias} and $\varepsilon_{scatter}$) and composite error ($\varepsilon_{composite}$) using data from the validation datasets (except the Van Noorloos and Boers experiments) with H_{rms} as the validation variable (the only common variable in all the experiments). This will give an estimate of the optimal gamma values based on a wide array of data which can be compared to the result obtained from the calibration.

Secondly, the performance of the ADA formulation (using the calibrated parameters from Section 3) will be assessed and compared

Table 2
Optimal gamma settings for calibration cases.

Series	Calibration variables	γ_b			γ_r		
		All	Pre-bar	Post-bar	All	Pre-bar	Post-bar
Boers 1A	H_{rms}	0.49	0.49	0.52	0.36	–	0.33
	Qb	0.52	0.52	0.52	0.30	–	0.30
	H_{rms}&Q_b	0.52	0.52	0.55	0.30	–	0.30
Boers 1B	H_{rms}	0.49	0.49	0.49	0.33	–	0.33
	Qb	0.52	0.49	0.55	0.30	–	0.30
	H_{rms}&Q_b	0.52	0.49	0.55	0.30	–	0.30

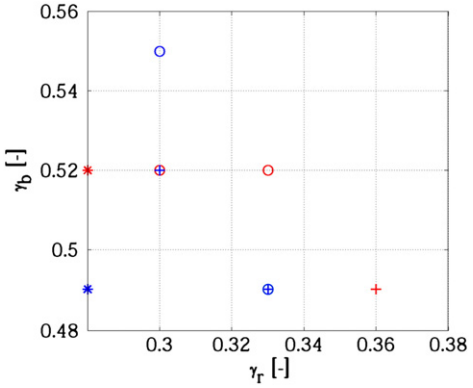

Fig. 6. Location of error distribution minima for calibration runs using data from all wave gauges (+), only the pre-bar wave gauges (○) and only the post-bar wave gauges (*). Data from Boers 1A is shown in red and Boers 1B is shown in blue. Since the pre-bar data is independent of γ_r, it is shown along the γ_b axis for illustration. (N.B. some points overlie others).

Table 3
Optimal gamma settings for sensitivity analysis.

Series	α	γ_b	γ_r	$\varepsilon_{composite}(H\&Q_b)$
Boers 1A	0.60	0.58	0.39	0.121
	0.80	0.55	0.33	0.079
	1.00	*0.52*	*0.30*	*0.065*
	1.20	0.55	0.27	0.088
	1.40	0.58	0.24	0.096
	1.60	0.49	0.27	0.137
Boers 1B	0.60	0.55	0.39	0.155
	0.80	0.52	0.33	0.097
	1.00	*0.52*	*0.30*	*0.067*
	1.20	0.52	0.27	0.086
	1.40	0.49	0.24	0.119
	1.60	0.46	0.24	0.156

Table 4
Field validation datasets and cases.

Dataset	Case	Bathymetry	ξ (−)
Ebersole and Hughes (1987)	D41400	Mobile barred beach	0.15
"	D41510	"	0.13
"	D50955	"	0.26
"	D51055	"	0.24
"	D51352	"	0.26
"	D51525	"	0.29
"	D60915	"	0.24
"	D61015	"	0.37
"	D61300	"	0.33
Hotta and Mizuguchi (1980)	HotMiz	Mobile barred beach	0.24

with the Rv93 formulation (calibrated by Roelvink, 1993) using the composite error given in Eq. (20) in addition to the Brier skill score (BSS) (Murphy and Epstein, 1989), given as:

$$\varepsilon_{bss} = 1 - \frac{\mathrm{var}(c-m)}{\mathrm{var}(m)}. \tag{21}$$

BSS values equal to 1 indicates perfect skill, 0 indicates no skill and negative values indicate very poor skill. The errors given by Eqs. (16) and (17) are calculated for H_{rms} using the entire validation dataset. Given that there are limited measurements of Q_b, from the datasets named in Table 4 and Table 5, this variable is compared using error statistics only for the Boers dataset where measured data are available and presented comparatively otherwise.

4.3. Results

4.3.1. Sensitivity of calibration parameter values

Fig. 8 shows results for the ε_{bias}, $\varepsilon_{scatter}$ and $\varepsilon_{composite}$ for H_{rms} using data from the validation cases. The optimal values of γ_b and γ_r in this case are shown to be 0.49 and 0.34 respectively, with the calibration parameter values of γ_b and γ_r also shown for comparison. Interestingly, despite the different datasets used to obtain the optimal values for γ_b and γ_r, this result is in agreement with those obtained from the calibration with only the Boers dataset where H_{rms} is used as the calibration variable (shown in Table 2). This demonstrates that the calibration values of γ_b and γ_r are insensitive to the source of data. Given the similarity of the calibration result for the H_{rms} calibration variable, we can hypothesise that the calibration result for the $H_{rms}\&Q_b$ variable combination would also lie in the same trough and would therefore be widely applicable to different types of field and laboratory cases as well.

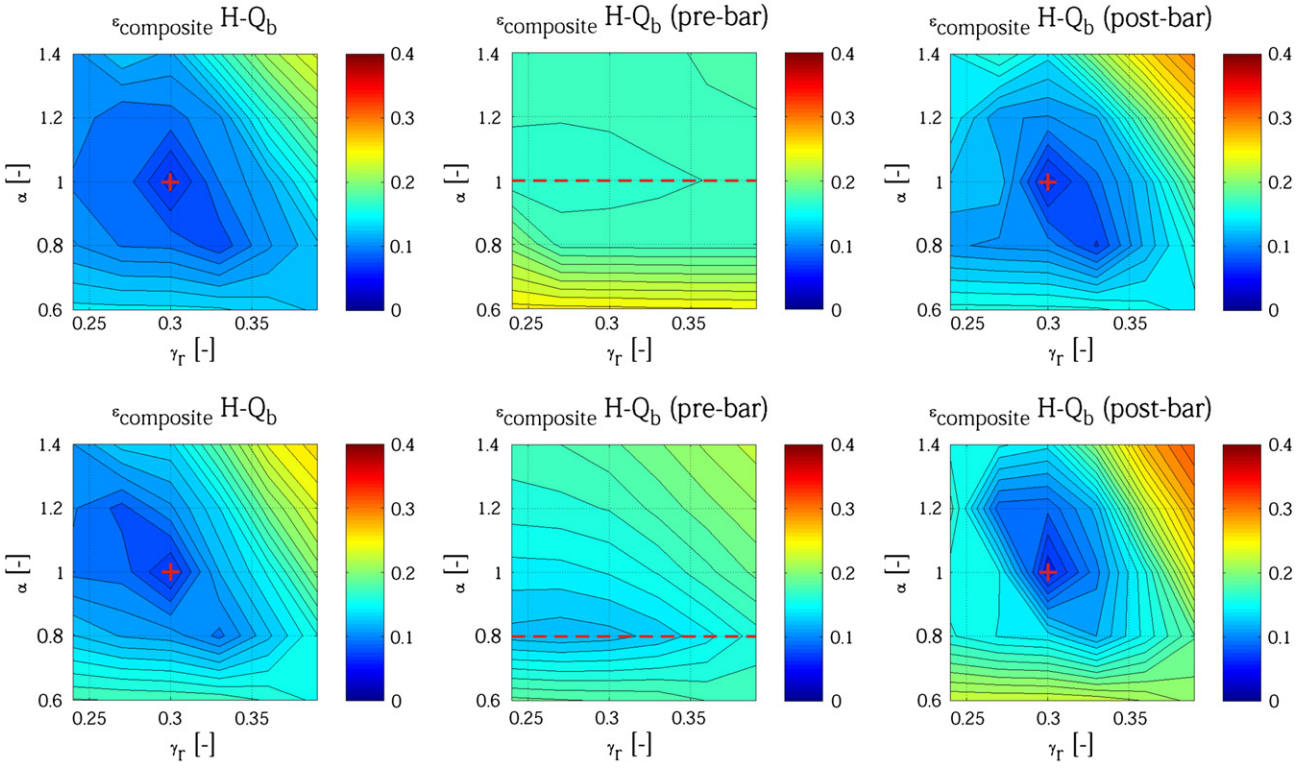

Fig. 7. Composite error distribution for the $H_{rms}\&Q_b$ pair, $\varepsilon_{composite}(H_{rms}\&Q_b)$ from case Boers 1A (top row) and Boers 1B (bottom row), for all wave gauge locations (left column), pre-bar wave gauges (centre column) and post-bar wave gauge locations (right column). Error distribution values (colour scale) are plotted against the breaking intensity, α (vertical axis) and the reformation parameter, γ_r (horizontal axis). Nodes (red +) and axes (red —) of minima are highlighted.

Table 5
Laboratory Validation Experiments and Cases.

Experiment	Case	Bathymetry	ξ (−)
Van der Meer (1990)	TST007	Fixed stepped slope	0.61
"	TST015	"	0.49
"	TST110	"	0.37
"	TST12	"	0.52
"	TST13	"	0.38
"	TST212	"	0.38
"	TST216	"	0.53
"	TST322	"	0.35
Stive (1985)	MS40A	Fixed plane slope	0.10
"	MS10A	"	0.15
Battjes and Janssen (1978)	BJ2	Fixed plane slope	0.24
"	BJ3	"	0.30
"	BJ4	"	0.26
"	BJ11	"	0.26
"	BJ12	"	0.27
"	BJ13	"	0.29
"	BJ14	"	0.26
"	BJ15	"	0.23
LIP11D (1995)	1A0708	Mobile barred slope	0.27
"	1B0607	"	0.23
"	1 C0706	"	0.41
"	2A0708	"	0.26
"	2B0708	"	0.20
"	2 C0708	"	0.40
"	2E0708	"	0.20
Van Noorloos (2003)	C1	Fixed plane slope	0.27
"	C2	"	0.22
"	C3	"	0.19
"	D1	"	0.23
"	D2	"	0.19
"	D3	"	0.16
Boers (1996)	1 C	Fixed barred slope	0.40

4.3.2. Prediction of short wave height

Results of the cross-shore RMS short wave height transformation for all 42 validation cases are shown in Fig. 9, Fig. 10 and Fig. 11 (including all field data and laboratory experiments). These plots show that the ADA model is capable of qualitatively representing the measured data quite well for the different wave conditions. Wave dissipation is captured quite well over varying nearshore bathymetry. In the Van der Meer cases, the ADA model predicts increased wave height reduction after the abrupt step in the bathymetry compared to the RV93 formulation, which more closely fits the measured data. In the Battjes and Janssen plane slope cases, the ADA formulation over-predicts the nearshore RMS short wave height slightly more than the Rv93 formulation. In most cases, the ADA formulation predicts equivalent or slightly lower RMS short wave heights in the nearshore than the Rv93 formulation.

Quantitatively, there is very little difference between the results of the ADA and Rv93 formulations. Table 6 below shows the mean BSS and $\varepsilon_{composite}$ values for the RMS short wave heights predicted by both breaker formulations. The breaker formulation that scores the highest on BSS values and the lowest on $\varepsilon_{composite}$ values is shown to be better than the other. In terms of the BSS, the Rv93 formulation is more-or-less similar to the ADA formulation (only a slight difference of 1.18%) while according to the composite error, the ADA formulation performs better than the Rv93 formulation (a difference of 13.8%).

The validation test cases, however, affirm that the ADA breaker model, using the calibration values of γ_b and γ_r, is capable of quantitatively and qualitatively representing the wave breaking process fairly accurately.

4.3.3. Prediction of fraction of breaking waves

While the RMS short wave height transformation is quite similar using both the Rv93 and the ADA breaker model, there are distinct differences in the results for the fraction of breaking waves, which we shall now address. From the 3 Boers cases where data for Q_b is available, two were used for the calibration of the model (cases 1A and 1B) and one in the validation (case 1 C). The results of the time-averaged Q_b for these cases are shown in Fig. 12. Here it can be seen from the measured data that in all cases wave breaking sharply increases at the nearshore bar and the level of breaking is sustained going into the trough. For cases 1A and 1B, there is a sudden dip in Q_b around the centre of the trough, where presumably waves are reforming. For case 1C, given a lower incident wave height and longer wave period than for cases 1A and 1B (refer to Table 1 in Model Calibration section), the level of breaking is lower at the bar but is fully maintained over the entire area of the trough (given longer incident waves). In all three cases, Q_b sharply increases again at the end of the trough and maintains a high level of breaking over the inner surf zone toward the shoreline.

The Q_b plots in Fig. 12 show that the ADA formulation qualitatively describes the measured data fairly well. Although used in the calibration process, the results from the ADA formulation for cases 1A and 1B clearly show two main breakpoints (at the bar and at the end of the trough) and a dip in Q_b around the centre of the trough as shown in the measured data. Even the results for the validation case of 1C show that breaking is maintained over the trough. The Rv93 formulation fails to correctly describe the pattern of breaking after the two main breakpoints as Q_b values fall close to zero after these points, which greatly under-predicts the occurrence of breaking. The mean BSS and $\varepsilon_{composite}$ Q_b values for the three Boers cases are shown in Table 6. The ADA formulation clearly exhibits greater skill and lower relative error than the Rv93 breaker model for Q_b.

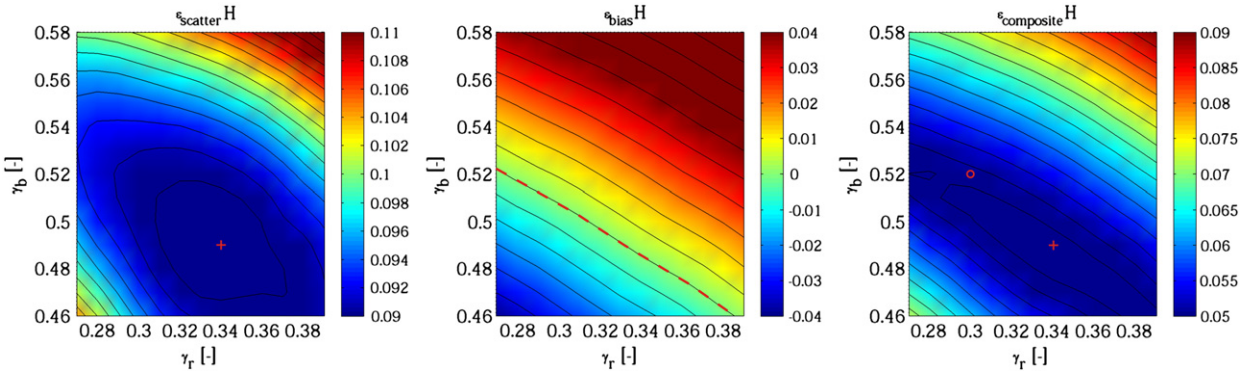

Fig. 8. RMS short wave height raw scatter error distribution, $\varepsilon_{scatter}(H_{rms})$ (left), raw bias error distribution, $\varepsilon_{bias}(H_{rms})$ (centre) and composite error distribution, $\varepsilon_{composite}(H_{rms})$ (right) using data from validation cases. Error distribution values (colour scale) are plotted against the breaker parameter, γ_b (vertical axis) and the reformation parameter, γ_r (horizontal axis) with corresponding nodes (red +) and axes (red —) of minima shown. The calibration parameter values of γ_b and γ_r is shown for reference (red ○).

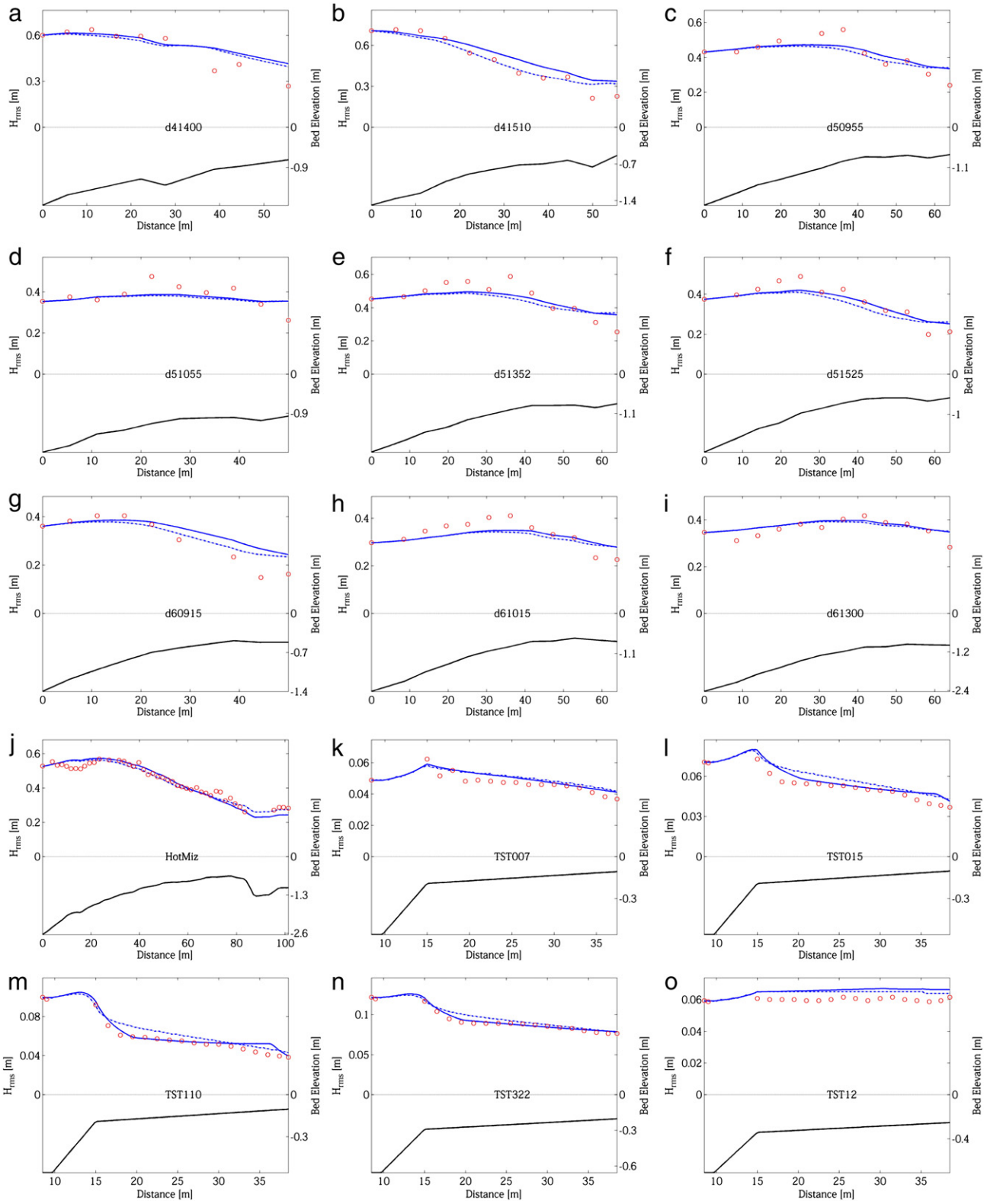

Fig. 9. Cross-shore variation of RMS short wave height, H_{rms}, for the wave cases of Duck '85 (panels a–i), Hotta and Mizuguchi (panel j), and Van der Meer (panels k–o). Measured data (red ○) is compared with the results obtained using the ADA (blue —) and Rv93 (blue —) breaker formulations. Bathymetry (black —) is shown below the wave height plots. (N.B. two different vertical scales).

Fig. 13 shows the results of the cross-shore variation in Q_b for some of the validation cases. Because of the absence of measured data, only 18 cases are shown for comparison of the predicted Q_b using the ADA and Rv93 breaker models. For these cases, the ADA breaker model is shown to predict higher and more sustained breaking in shallow water compared to the Rv93 formulation. An important feature of the ADA model is highlighted in cases where there is varied bathymetry (e.g. the Van der Meer and Delta Flume cases), whereby wave breaking does not stop prematurely after abrupt changes in bathymetry as with the Rv93 model, which is what we would also expect in nature.

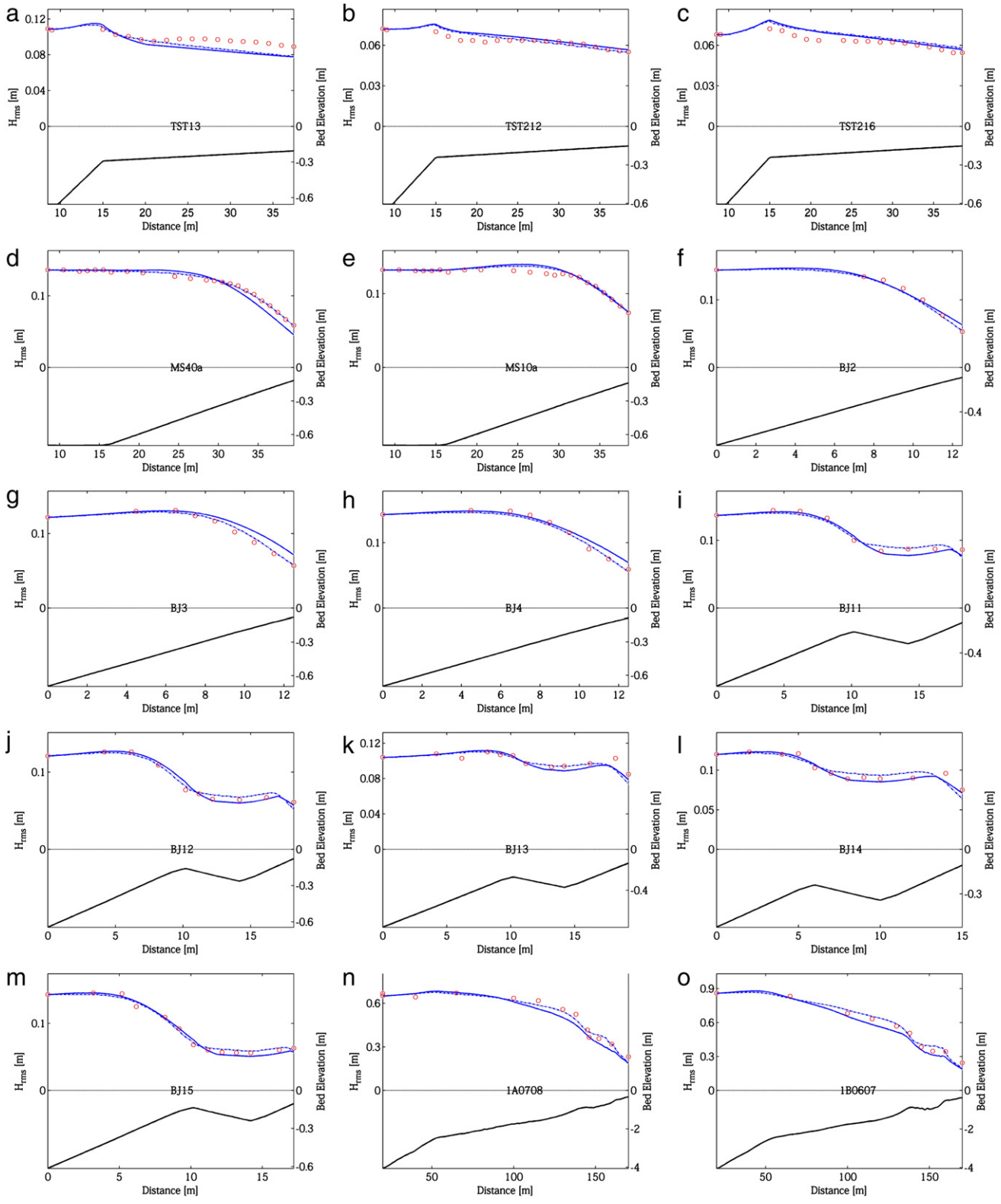

Fig. 10. Cross-shore variation of RMS short wave height, H_{rms}, for the wave cases of Van der Meer (panels a–c), Stive (panels d–e), Battjes and Janssen (panels f–m), and LIP11D (panels n–o). Measured data (red ○) is compared with the results obtained using the ADA (blue —) and Rv93 (blue —) breaker formulations. Bathymetry (black —) is shown below the wave height plots. (N.B. two different vertical scales).

5. Discussion

In the calibration, we recommended default parameter values for γ_b and γ_r, based on the results obtained using the $H_{rms}\&Q_b$ variable combination using all wave gauges. We will discuss following why we choose this as prescribed model settings from the calibration and how other model settings could affect these values. We also discuss some of the theory behind the model and mention possible improvements. Lastly, we briefly mention some of the possible implications of using the ADA breaker model.

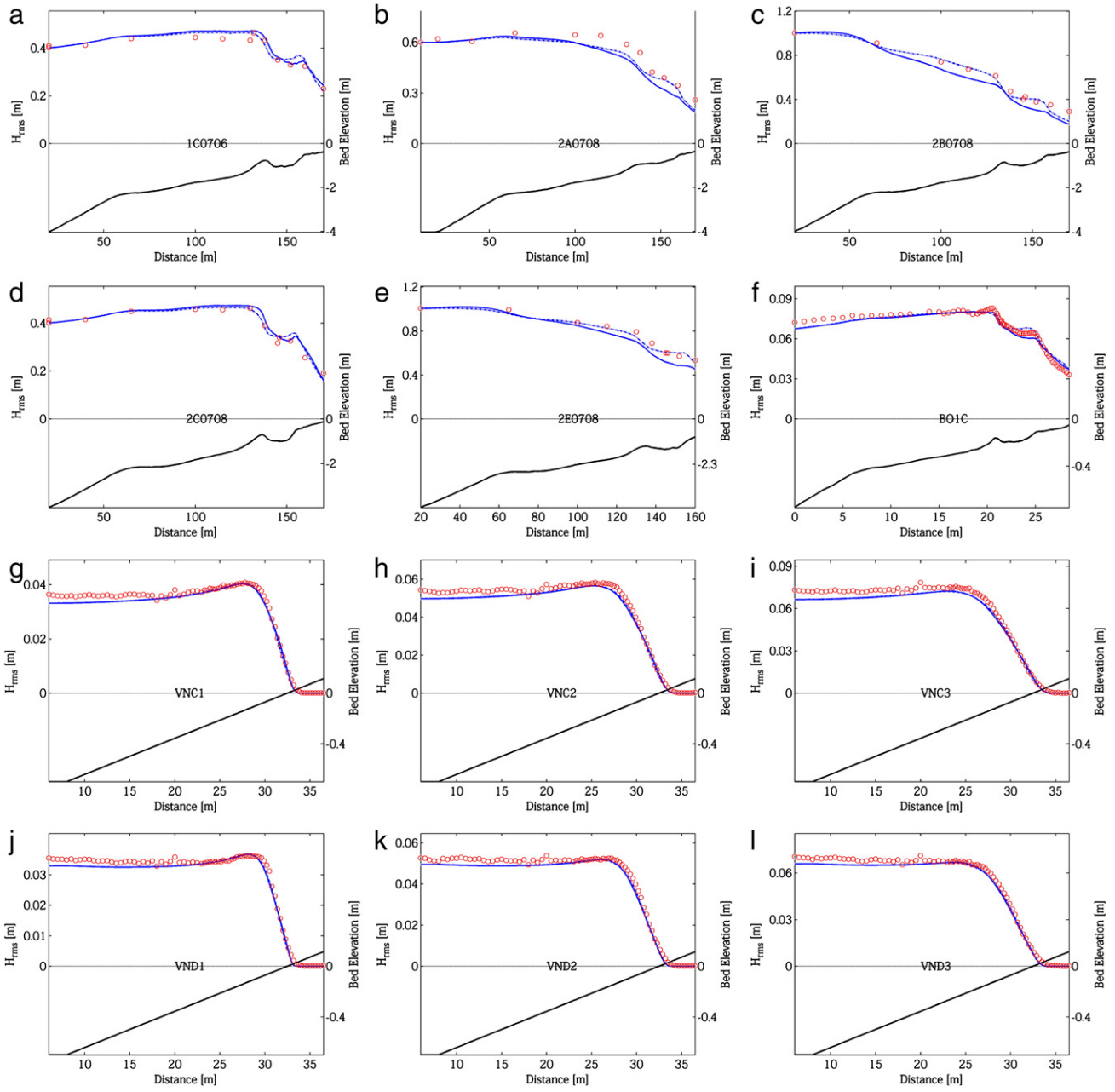

Fig. 11. Cross-shore variation of RMS short wave height, H_{rms}, for the wave cases of LIP11D (panels a–e), Boers 1C (panel f), and Van Noorloos (panels g–l). Measured data (red ○) is compared with the results obtained using the ADA (blue —) and Rv93 (blue —) breaker formulations. Bathymetry (black —) is shown below the wave height plots. (N.B. two different vertical scales).

5.1. Calibration of the ADA model

5.1.1. Variable combinations

Using various calibration variables (H_{rms} and Q_b) results in multiple locations where error distribution minima occur as shown in Fig. 6. The presence of scatter within these minima signifies that there is either natural variance in wave breaking limits (which implies that wave breaking is not completely deterministic) or that there are additional processes which are not accounted for by either the ADA model or other formulations within the XBeach code (for example the linear wave action balance equations). It is difficult to pinpoint exactly where this discrepancy lies, but it is not uncommon to modelling in general. The question then arises as to whether we should ignore certain variables to essentially limit this uncertainty to one calibration variable, either H_{rms} or Q_b. Given that the processes of wave height decay through energy dissipation and the occurrence of wave breaking are coupled in nature, we can argue that both H_{rms} and Q_b should have influence in the model calibration, especially since both are direct outputs of the ADA model itself. Although the composite error for H_{rms} and Q_b can be obtained individually, the most representative error comes from the combination of both variables.

Table 6
Mean errors for the ADA and Rv93 formulations.

Variable	Rv93	ADA	% Difference
Mean BSS (H_{rms})	0.7464	0.7376	1.18
Mean $\varepsilon_{composite}(H_{rms})$	0.0778	0.0669	13.8
Mean BSS (Q_b)	0.4465	0.8536	91.1
Mean $\varepsilon_{composite}(Q_b)$	0.4654	0.1844	60.4

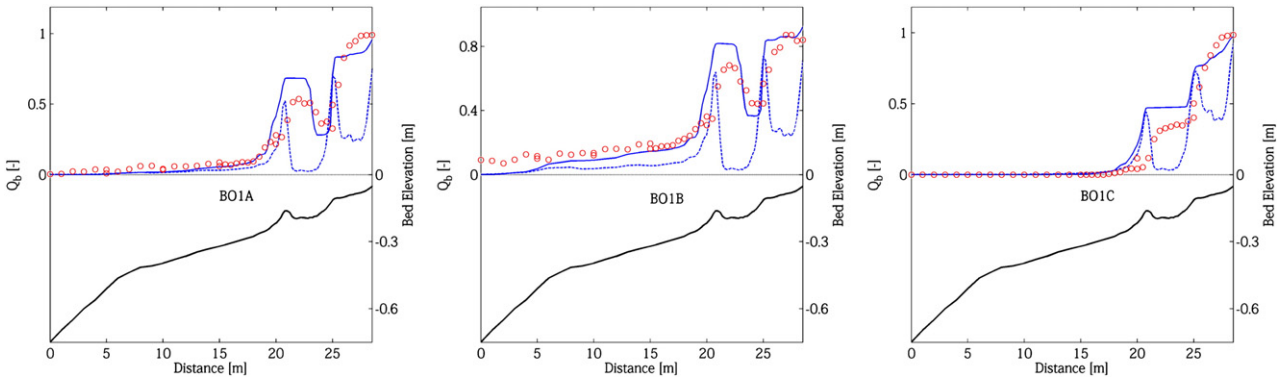

Fig. 12. Cross-shore variation of fraction of breaking waves, Q_b, for all wave cases of Boers. Measured data (red ○) is compared with the results obtained using the ADA (blue ——) and Rv93 (blue ——) breaker formulations. Bathymetry (black ——) is shown below the Q_b plots. (N.B. two different vertical scales).

5.1.2. Pre- and post-breaker bar

Though wave breaking may start early in the flume, the point where it is able to reform tends to lie further inshore of the pre-bar section. Given the limited number of waves reforming in the pre-bar section of the flume, it therefore may not fully satisfy all the conditions inherently required to calibrate the ADA model, particularly for γ_r. For this reason, separating the flume into two areas gives us the opportunity to observe differences which occur when we look at all wave gauges or only those in the post-bar breaker zone. A slight drawback to this approach is that the number of wave gauges in the post-bar zone is only half of the total number of wave gauges, 36 in all, but it can be considered a reasonable number to obtain dependable error statistics from the calibration. The results show that γ_r tends to be undefined in the pre-bar area, but definitive results are obtained for γ_r in the post-bar area. However, for practical purposes the estimation of wave heights in the complete cross-shore area is of general interest, therefore the calibration results using all wave gauges is preferred. Considering the results shown in Table 2 for γ_b and γ_r, the difference between values obtained by using all wave gauges and only those in the post-bar area is, in any case, marginal.

5.2. Model theory

5.2.1. Deterministic approach

Most existing breaker models employ a probabilistic approach to model wave breaking which is usually applicable to wave averaged models. The ADA breaker model, being wholly deterministic, is clearly not similar to a probabilistic model in theory. It can only be implemented in time-dependent numerical models, and in fact, it is quite crude in its assumption that breaking starts and ends at a predefined points. In order to include random variations in breaking, the ADA model therefore becomes reliant on the natural randomness within the wave height distribution itself.

5.2.2. History and advection of breaking

Wave breaking is advected shoreward with the speed of the individual wave in the ADA breaker model. This is similar in theory to the roller energy dissipation model (Deigaard, 1993). The ADA model therefore implicitly tracks the breaking of an individual wave within the wave group. The history of wave breaking is a key factor in determining the current state of breaking at an upwind point in the model domain. Waves which are previously breaking are assumed to continue breaking until the wave becomes stable and reforms. Therefore the ADA breaker model can describe breaking patterns in situations where wave breaking is occurring repetitively (as shown in Fig. 1). The fraction of breaking waves shown for the Boers test cases indicates that this concept is proven in nature and predicted well by the ADA breaker model. However, additional test cases with measurements of Q_b should be used to augment the three Boers cases. It should also be noted that the ADA breaker model also performs equally well on beaches with a single breaking zone, as shown in the wave cases of Van Noorloos and Battjes and Janssen.

5.2.3. Possible improvements

Further modifications can be made to the ADA formulation to account for the possible variance of γ_b and γ_r values, for example, by constructing p.d.f.'s for each parameter. Such an approach would require laboratory testing and, unfortunately, there is very little published literature at this time regarding laboratory or prototype measurements of γ_r. It is possible that the default values γ_b and γ_r, which are based on indirect calibration with H_{rms} and Q_b, could change slightly if determined from direct measurements. It is therefore recommended that wave-by-wave data for B, γ_b and γ_r be gathered from future flume experiments.

5.3. Possible implications

In the Model Validation section, the ADA breaker model showed good skill in predicting short wave height transformation over various cross-shore bathymetries. While there is no significant improvement in this area over existing models (Rv93), the difference is shown to be in the prediction of Q_b. The latter is an important variable because it can influence radiation stress gradients within the surf zone. This stems from the roller concept, whereby energy taken from the wave during breaking and is transferred to the roller, which is an additional source of radiation stress than that of the short waves themselves (Deigaard, 1993). The distinct difference between the predicted Q_b using the ADA breaker model and the Rv93 formulation could possibly lead to differences in the prediction of low frequency wave forcing by wave groups; low frequency wave generation by wave breaking; wave-induced currents and circulation patterns; and wave setup over complex bathymetries. This should be the focus of further research.

6. Conclusions

In this paper an advective-deterministic approach to model wave energy dissipation through breaking is proposed. In this model, the dissipation of wave energy is equivalent to that in a hydraulic jump and breaking only occurs within the specific upper limit of a breaker parameter γ_b and lower limit of a reformation parameter, γ_r. The property that a wave is breaking or not is advected shoreward with the individual wave celerity. The model is calibrated using the results of short wave height and fraction of breaking waves from two cases of a controlled flume experiment (Boers, 1996), from which optimal values for γ_b and γ_r are obtained as 0.52 and 0.30 respectively. The optimal parameter values for γ_b and γ_r is found to be the same also when using a larger dataset.

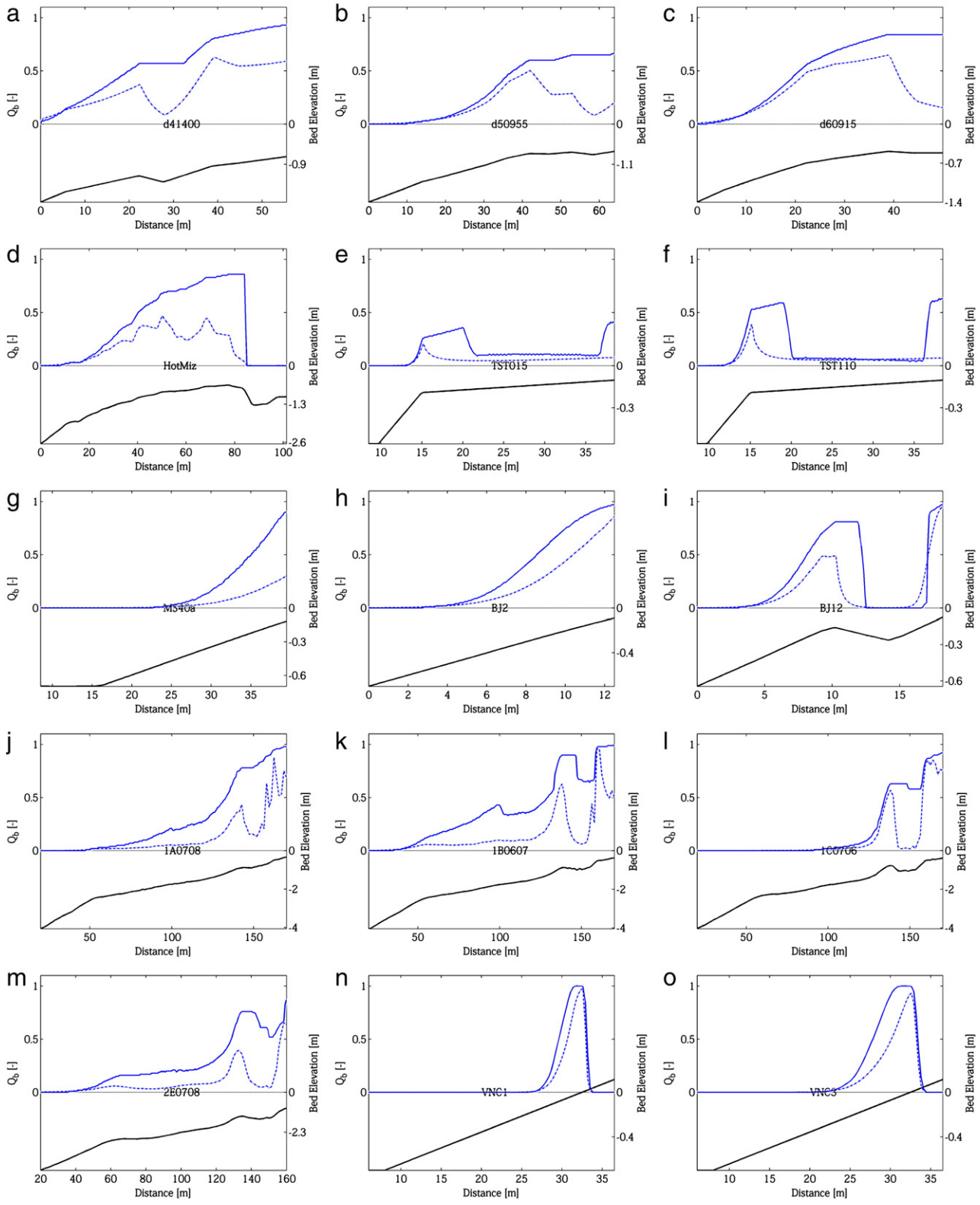

Fig. 13. Cross-shore variation of fraction of breaking waves, Q_b, for the wave cases of Duck '85 (panels a–b), Hotta and Mizuguchi (panel c), Van der Meer (panels d–e), Stive (panel f), Battjes and Janssen (panel i–k), LIP11D (panels l–o) and Van Noorloos (panels n–o). Results obtained using the ADA formulation (blue ——) is compared with the results of the Rv93 formulation (blue ——). Bathymetry (black ——) is shown below the Q_b plots. (N.B. two different vertical scales).

The ADA model is validated using measured data from 10 field experiments and 32 flume experiments and is also compared to the results using the breaker model of Roelvink (1993). The results show that the ADA model is very capable of representing cross-shore short wave height transformation. The ADA breaker model has a similar BSS score as the Roelvink (1993) breaker model for representing the cross-shore short wave height; however, it has a lower composite error (a combination of the bias and scatter) than the Roelvink (1993)

breaker model. Most notably, the prediction of the fraction of breaking waves is markedly improved using the ADA breaker model over the Roelvink (1993) breaker model, as the former is able to sustain breaking for longer periods over sudden changes in bathymetry. Given the differences in the predictions of the fraction of breaking waves (and therefore radiation stress gradients), we can expect that this approach to wave breaking has the potential to give different model results for other nearshore processes such as the generation and shoaling of low frequency waves and nearshore circulation over complex bathymetries.

Acknowledgements

The Research reported in this paper has been made possible through the support of the European Community's Seventh Framework Program under grant agreement no. 202798 (MICORE Project); Deltares Delft Cluster project 5.20: North Sea; and Deltares Strategic Research 1202362. The authors would like to thank both anonymous reviewers for their constructive comments and feedback on the manuscript.

References

Baldock, T.E., Holmes, P., Bunker, S., van Weert, P., 1998. Cross-shore hydrodynamics within an unsaturated surf zone. Journal of Coastal Engineering 34, 173–196.
Battjes, J.A., 1974. Surf similarity. Proc. 14th Int. Conf. Coastal Eng, pp. 1419–1438.
Battjes, J.A., Janssen, J.P.F.M., 1978. Energy loss and set-up due to breaking in random waves. Proc. 16th Int. Conf. Coastal Eng, pp. 569–587.
Battjes, J.A., Stive, M.J.F., 1985. Calibration and verification of a dissipation model for random breaking waves. Journal of Geophysical Research 90, 9159–9167.
Boers, M., 1996. Simulation of a surf zone with a barred beach; Report 1: wave heights and wave breaking. Comm. on Hydraulic and Geo. Eng., No. 96–05. Delft Univ. of Technology.
Dally, W.R., 1990. Random breaking waves: a closed-form solution for planar beaches. Journal of Coastal Engineering 14, 233–263.
Dally, W.R., 1992. Random breaking waves: field verification of a wave-by-wave algorithm for engineering application. Journal of Coastal Engineering 16, 369–397.
Dally, W.R., Dean, R.G., Dalrymple, R.A., 1985. Wave height variation across beaches of arbitrary profile. Journal of Geophysical Research 90 (C6), 11,917–11,927.
Deigaard, R., 1993. A note on the three dimensional shear stress distribution in a surf zone. Journal of Coastal Engineering 20, 157–171.
Ebersole, B.A., Hughes, S.A., 1987. Duck85 photopole experiment. U.S. Army Waterways Experiment Station, misc. paper CERC-87-18, Vicksburg, MS. .
Elfrink, B., Baldock, T., 2002. Hydrodynamics and sediment transport in the swash zone: a review and perspectives. Journal of Coastal Engineering 45, 149–167.
Horikawa, K., Kuo, C., 1966. A study of wave transformation inside the surf zone. Proc. of the 10th Int. Conf. Coastal Eng, pp. 217–233.
Hotta, S., Mizuguchi, M., 1980. A field study of waves in the surf zone. Coastal Eng. in Japan, Vol. XXIII. Japan Soc. of Civil Engineers, Tokyo.
Le Mehaute, B., 1962. On non-saturated breakers and the wave run-up. Proc. 8th Int. Conf. Coastal Eng, pp. 1178–1191.
Longuet-Higgins, M.S., Stewart, R.W., 1962. Radiation stress and mass transport in gravity waves, with application to surf beats. Journal of Fluid Mechanics 13, 481–504.
Mase, H., lwagaki,, Y., 1982. Wave height distributions and wave grouping in surf zone. Proc. 18th Int. Conf. Coastal Eng, pp. 58–76.
Murphy, A.H., Epstein, E.S., 1989. Skill scores and correlation coefficients in model verification. Monthly Weather Review 117, 572–581.
Roelvink, J.A., 1993. Dissipation in random wave groups incident on a beach. Journal of Coastal Engineering 19, 127–150.
Roelvink, J.A., Reniers, A.J.H.M., 1995. LIP 11D delta flume experiments. Data Report H2130. Delft Hydraulics, Delft.
Roelvink, J.A., Reniers, A.J., van Dongeren, A.R., van Thiel de Vries,, J.S.M., McCall, R., Lescinski, J., 2009. Modeling storm impacts on beaches, dunes and barrier islands. Journal of Coastal Engineering. doi:10.1016/j.coastaleng.2009.08.006.
Schaffer, H.A., Svendsen, I.A., 1988. Surf beat generation on a mild slope beach. Proc. 21st Int. Conf. Coastal Eng, pp. 1058–1072.
Stive, M.J.F., 1985. A scale comparison of waves breaking on a beach. Journal of Coastal Engineering 9, 151–158.
Symonds, G., Black, K.P., 1991. Numerical simulation of infragravity response in the nearshore. Proc. 10th Australasian Coastal and Ocean Eng. Conf., Auckland, pp. 339–344.
Symonds, G., Huntley, D.A., Bowen, A.J., 1982. Two-dimensional surf beat. Long wave generation by a varying breakpoint. Journal of Geophysical Research 80, 492–498.
Thornton, E.B., Guza, R.T., 1983. Transformation of wave height distribution. Journal of Geophysical Research 88, 5925–5938.
van der Meer, J.W., 1990. Golfhoogtes van brekende golven op een flauw talud (Wave heights for breaking waves on a flat slope, in Dutch). Delft Hydraulics report no. H462-IV, Delft.
van der Westhuysen, A.J., 2010. Modeling of depth-induced wave breaking under finite depth wave growth conditions. Journal of Geophysical Research 115, C01008.
van Dongeren, A.R., Battjes, J.A., Janssen, T.T., van Noorloos, J.C., Steenhauer, K., Steenbergen, G., Reniers, A., 2007. Shoaling and shoreline dissipation of low-frequency waves. Journal of Geophysical Research 112, C02011.
van Noorloos, J.C., 2003. Energy transfer between short wave groups and bound long waves on a plane slope. MSc. Thesis, Delft Univ. of Technology.